J Electr Eng Technol Vol. 8, No. 6: 1439-1450, 2013
http://dx.doi.org/10.5370/JEET.2013.8.6.1439

ISSN(Print) 1975-0102
ISSN(Online) 2093-7423

Neuro-Fuzzy Control of Interior Permanent Magnet Synchronous Motors: Stability Analysis and Implementation

Dong Quang Dang*, Nga Thi-Thuy Vu*, Han Ho Choi* and Jin-Woo Jung†

Abstract – This paper investigates a robust neuro-fuzzy control (NFC) method which can accurately follow the speed reference of an interior permanent magnet synchronous motor (IPMSM) in the existence of nonlinearities and system uncertainties. A neuro-fuzzy control term is proposed to estimate these nonlinear and uncertain factors, therefore, this difficulty is completely solved. To make the global stability analysis simple and systematic, the time derivative of the quadratic Lyapunov function is selected as the cost function to be minimized. Moreover, the design procedure of the online self-tuning algorithm is comparatively simplified to reduce a computational burden of the NFC. Next, a rotor angular acceleration is obtained through the disturbance observer. The proposed observer-based NFC strategy can achieve better control performance (i.e., less steady-state error, less sensitivity) than the feedback linearization control method even when there exist some uncertainties in the electrical and mechanical parameters. Finally, the validity of the proposed neuro-fuzzy speed controller is confirmed through simulation and experimental studies on a prototype IPMSM drive system with a TMS320F28335 DSP.

Keywords: Interior permanent magnet synchronous motor (IPMSM), Linear matrix inequality (LMI), Neuro-fuzzy control (NFC), Robustness, Speed control, System uncertainties

1. Introduction

The permanent magnet synchronous motor (PMSM) has been extensively used in variable-speed motor drives such as electric vehicles, home appliances, military or medical equipment, machine tools, and industrial robots because of its wide speed range operation and high power density [1-4]. Depending on the position of the permanent magnet on the rotor, the PMSM can be mainly classified into two types: surface-mounted PMSM (SPMSM) and interior PMSM (IPMSM). It is well-known that the IPMSM is more difficult to control due to more complex dynamic model, but has better performance (i.e., a wider speed range operation capability due to flux weakening control and a higher torque generation capability due to inherent saliency) than the SPMSM. Thanks to these attractive advantages, the IPMSM is gaining more and more attention in industrial and home appliance application areas. However, it is complicated to precisely control the IPMSM because of the nonlinearities due to nonlinear properties resulting from the magnets and cross-coupling between the state variables (i.e., the *dq*-axis currents and speed) in dynamic model equations. Also, there always exist system uncertainties such as motor parameter variations and unknown external disturbances. Therefore, the robust control design requirements should be satisfied, which are insensitive to the uncertainties mentioned previously. Consequently, the classical linear control schemes based on time-invariant system model, e.g., the PI controller [5], cannot achieve a good tracking performance.

To solve these difficulties, many advanced control approaches have been presented such as feedback linearization control [6], adaptive backstepping control [7], optimal control [8], predictive control [9-10], etc. In [6], the control performance of the feedback linearization algorithm is not satisfactory because its property is sensitive to parameter uncertainties and external disturbances. In [7], the design procedure of the adaptive backstepping control methods looks complicated since many parameters are adapted. In [8-10], the control algorithms of the IPMSMs are comparatively simple because the *d*-axis current reference is set to zero. However, the torque of the IPMSMs cannot be maximized by making the reluctance torque be zero. Also, the fuzzy control schemes [11-12] have been introduced to make up for the nonlinearities of IPMSM system. It is easy to see that the control scheme becomes complex and difficult to be designed as the number of fuzzy rules increases. The sliding mode control approach [13-14] has its favorable advantage which is insensitive to parameter uncertainties and external disturbances. However, the robustness of this control method can be guaranteed only within the bounds of the uncertainties, and it still suffers from a chattering problem. Beside the above control methods, many papers have concentrated to investigate the effects of both the mechanical and electrical parameter variations on the servo

† Corresponding Author: Division of Electronics and Electrical Engineering, Dongguk University-Seoul, Korea. (jinwjung@dongguk.edu)
* Division of Electronics and Electrical Engineering, Dongguk University-Seoul, Korea.
Received: June 1, 2013; Accepted: August 12, 2013

IPMSM drives [15-16]. Some outstanding methods have been used to estimate the motor parameters, such as an online method [15] and a terminal sliding-mode observer method [16]. These papers implied that the control scheme can significantly improve the system performance, if the motor parameters are accurately estimated and then directly used to design the controllers.

Recently, the intelligent control methods such as fuzzy logic control, neural network control, neuro-fuzzy control (NFC) have received a lot of attentions since these controllers do not need an exact mathematical model of the system and can achieve high performance. Especially, the NFC is a combination of the advantages of artificial neural network control and fuzzy logic control. That means the artificial neural network has learning ability that can acquire the appropriate information based on the data while the fuzzy logic control can reasonably characterize the input/output behaviors of an uncertain system. In [17-18], the NFC is applied to tune the PI gains for IPMSM drives. However, its parameter training is optimized offline. In [19-21], the NFC faces a burdensome computation because of using a huge number of membership functions and rules. This is a major constraint for industrial applications. Furthermore, the NFC algorithms of [22-23] are quite complex when the reference models of the online self-tuning algorithm are utilized.

This paper introduces a robust neuro-fuzzy speed control strategy that can accurately track the speed reference trajectory of IPMSM in spite of system uncertainties. The proposed NFC method contains a state feedback control term and a NFC term. The former stabilizes the system error dynamics and the latter makes up for nonlinearities and uncertain factors. Furthermore, the maximum torque per ampere (MTPA) control is combined with the proposed controller to maximize the torque generation in the constant torque region. Unlike the previous online self-tuning algorithms [17-23] in which the quadratic cost function to be minimized includes only the speed error, the proposed control technique chooses the time derivative of the quadratic Lyapunov function as the cost function to be minimized. Thus, the global stability analysis can be simple and systematic. Furthermore, the design procedure of the online self-tuning algorithm is comparatively simplified to reduce a computational burden of the NFC. A rotor angular acceleration is attained through the disturbance observer. To prove the robustness of the proposed NFC scheme and the effects of two kinds of parameter variations, in both simulation and experimental studies, the results of the proposed NFC and the feedback linearization control (FLC) methods are presented under the mechanical parameters variations as well as the electrical parameters variations using Matlab/Simulink software and a prototype IPMSM drive system with a TMS320F28335 DSP, respectively. The results show that the proposed observer-based NFC scheme can attain better tracking control performance (i.e., less steady-state error, more robustness) than the observer-based FLC method even when there exist some uncertainties in the electrical and mechanical parameters.

2. Neuro-fuzzy Speed Controller Design and Stability Analysis

2.1 Mathematical model of IPMSM

In the synchronously rotating *dq* reference frame, where the *d*-axis is aligned with the rotor flux vector and the *q*-axis is always 90° ahead of the *d*-axis, a three-phase IPMSM can be modeled by the dynamic equations including system uncertainties [9] as

$$\begin{aligned}\dot{\omega} &= k_1 i_{qs} - k_2\omega + k_{11} i_{ds} i_{qs} - k_3 d_1(t)\\ \dot{i}_{qs} &= -k_4 i_{qs} - k_5\omega + k_6 V_{qs} - k_{10}\omega i_{ds} - k_6 d_2(t)\\ \dot{i}_{ds} &= -k_7 i_{ds} + k_8 V_{ds} + k_9\omega i_{qs} - k_8 d_3(t)\end{aligned} \tag{1}$$

where

$$k_1 = \frac{3}{2}\frac{1}{J}\frac{p^2}{4}\lambda_m,\ k_2 = \frac{B}{J},\ k_3 = \frac{p}{2J},\ k_4 = \frac{R_s}{L_{qs}},$$
$$k_5 = \frac{\lambda_m}{L_{qs}},\ k_6 = \frac{1}{L_{qs}},\ k_7 = \frac{R_s}{L_{ds}},\ k_8 = \frac{1}{L_{ds}},$$
$$k_9 = \frac{L_{qs}}{L_{ds}},\ k_{10} = \frac{L_{ds}}{L_{qs}},\ k_{11} = \frac{3}{2}\frac{1}{J}\frac{p^2}{4}(L_{ds} - L_{qs}),$$

ω is the electrical rotor speed; i_{ds} and i_{qs} are the *d*-axis and *q*-axis currents; V_{ds} and V_{qs} are the *d*-axis and *q*-axis voltages; T_L is the load torque; p is the number of poles; R_s, L_{ds}, L_{qs}, J, B, and λ_m are the nominal values of the stator resistance, *d*-axis inductance, *q*-axis inductance, rotor inertia, viscous friction coefficient, and magnetic flux, respectively; the disturbances $d_i(t)$ defined in [9] represent motor parameter uncertainties and unknown external load torque.

In this work, the speed controller design will be based on the assumptions and definitions described below:

Assumption 1: ω, i_{ds}, and i_{qs} are measurable.

Assumption 2: The desired speed ω_d and the disturbances $d_i(t)$ vary slowly for a sampling period [9-10].

Definition 1: The electrical angular acceleration is represented as

$$\beta = \dot{\omega} = k_1 i_{qs} - k_2\omega + k_{11} i_{ds} i_{qs} - k_3 d_1(t) \tag{2}$$

Definition 2: To produce the maximum torque per ampere (MTPA) of the stator current, the *d*-axis reference current is calculated [12-13] by

$$i_{dsd} = \frac{(L_{ds} - L_{qs})i_{qs}^2}{\lambda_m} \tag{3}$$

Definition *3:* The speed error, the *d*-axis current error, and the error vector are introduced as $\omega_e = \omega - \omega_d$, $i_{dse} = i_{ds} - i_{dsd}$, and $x = [\omega_e \quad \beta \quad i_{dse}]^{\mathrm{T}}$, respectively.

From the above *assumptions* and *definitions*, the dynamic Eq. (1) can be converted to the following form:

$$\dot{x} = Ax + B(u - f) \tag{4}$$

where

$$f = \begin{bmatrix} f_q & f_d \end{bmatrix}^T, u = \begin{bmatrix} k_1 k_6 & 0 \\ 0 & k_8 \end{bmatrix} \begin{bmatrix} V_{qs} \\ V_{ds} \end{bmatrix},$$

$$B = [B_1 \; B_2] = \begin{bmatrix} 0 & 0 \\ 1 & 0 \\ 0 & 1 \end{bmatrix}, A = \begin{bmatrix} 0 & 1 & 0 \\ -k_1 k_5 & -k_2 & 0 \\ 0 & 0 & -k_7 \end{bmatrix},$$

$$f_q = k_1 k_5 \omega_d + k_1 k_{10} \omega i_{ds} - k_{11}(\dot{i}_{ds} i_{qs} + i_{ds} \dot{i}_{qs}) + k_1 k_4 i_{qs} + k_1 k_6 d_2(t),$$

$$f_d = k_7 i_{dsd} - k_9 \omega i_{qs} + \dot{i}_{dsd} + k_8 d_3(t)$$

Note that the above state-space model (4) is considered to construct the proposed control law and requires the rotor angular acceleration information β which is usually immeasurable. Moreover, the functions f_q and f_d include the nonlinear terms and the uncertainty terms. Assume that there exists a constant parameter matrix $W^{*2r\times 1}$ such that

$$f = \mathrm{H} W^* \tag{5}$$

where $H^{2\times 2r}$ is a known function matrix, and r is a positive integer that denotes the number of fuzzy rules in the following subsection.

2.2 Neuro-fuzzy speed controller design

Let the control law u be decomposed as the state feedback control term u_{fb} and the adaptive compensating control term u_{nf}

$$u = u_{fb} + u_{nf} \tag{6}$$

First, the state feedback term design is based on a linear matrix inequality (LMI) condition. Assume that there is an existing pair of matrix solution (X, Y) that satisfies the following inequality

$$X > 0, \; AX - BY + XA^T - Y^T B^T < 0 \tag{7}$$

where $X \in R^{3\times 3}$ and $Y \in R^{2\times 3}$ are decision variables.

The gain matrix K of the state feedback term u_{fb} is obtained by

$$K = YX^{-1}, u_{fb} = -Kx \tag{8}$$

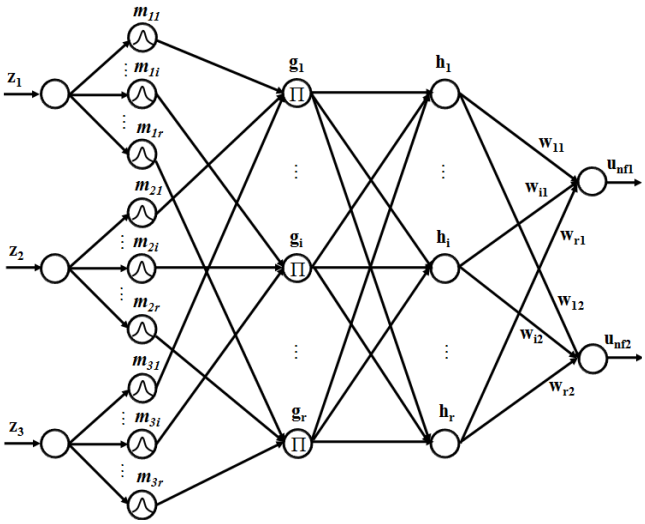

Fig. 1. Five-layer NFC with weight normalization

Then the NFC is applied to construct the adaptive compensating term that deals with f_q and f_d. Fig. 1 shows the structure of the NFC with weight normalization which consists of five basic layers. The first layer which is an input layer distributing the input variables to each of the nodes in the second layer is indicated. For the aim of reducing a computational burden, only three input signals z_j (j = 1, 2, 3) are considered: $z_1 = \omega$, $z_2 = i_{qs}$, and $z_3 = i_{ds}$. Layer 2 is a fuzzification layer and every node in this layer acts as the membership function. In this work, for easy implementation, the following Gaussian membership functions can be selected as

$$m_{ji} = \exp[-\frac{(z_j - \varepsilon_{ji})^2}{(\sigma_{ji})^2}], i = 1, 2, ..., r \tag{9}$$

where r is the number of fuzzy rules, ε_{ji} and σ_{ji} denote the center and the width of the membership function m_{ji}, respectively. Next, layer 3 is a rule layer and the output of every node in this rule layer is defined as

$$g_i = \prod_{j=1}^{3} m_{ji} \tag{10}$$

Layer 4 is a normalizing layer with r nodes and every node in this layer can be regarded as the normalized weight of each rule.

$$h_i = \frac{g_i}{\sum_{i=1}^{r} g_i} \tag{11}$$

Layer 5 is an output layer containing two nodes and each

output u_{nfk} (k =*1*, *2*) of the kth node is denoted as

$$u_{nfk} = \sum_{i=1}^{r} h_i w_{ik} \tag{12}$$

where w_{ik} are the adjustable parameter vectors. Finally, the adaptive compensating term is denoted as

$$\begin{aligned} u_{nf} &= \left[u_{nf1}\, u_{nf2} \right]^T = \mathrm{H} W \\ \mathrm{H} &= \begin{bmatrix} h_1\, h_2 \ldots h_r\ 0\ 0 \ldots 0 \\ 0\ 0 \ldots 0\ h_1\, h_2 \ldots h_r \end{bmatrix}, \\ W &= \left[w_{11}\, w_{21} \ldots w_{r1}\, w_{12}\, w_{22} \ldots w_{r2} \right]^T \end{aligned} \tag{13}$$

Then, the online self-tuning algorithm is utilized to update all parameters in real-time, and the object function to be minimized is defined as

$$E = \dot{x}^T P x \tag{14}$$

where $P=X^{-1}$. Based on the back-propagation learning rule that is computed recursively from the output layer backward to the input layer, the weights in the output layer are updated by

$$\begin{aligned} &\dot{w}_{ik} = -\eta_{ik} \frac{\partial E}{\partial w_{ik}} = -\eta_{ik} \frac{\partial E}{\partial \dot{x}^T} \frac{\partial \dot{x}^T}{\partial u_{nfk}} \frac{\partial u_{nfk}}{\partial w_{ik}} = -\eta_{ik} h_i B_k^T P x, \\ &\eta_{ik} > 0, \frac{\partial E}{\partial \dot{x}^T} = P x, \frac{\partial \dot{x}^T}{\partial u_{nfk}} = B_k^T, \frac{\partial u_{nfk}}{\partial w_{ik}} = h_i \end{aligned} \tag{15}$$

Then, the adaptive law can be expressed by

$$\begin{aligned} \dot{W} &= -E_w \mathrm{H}^T \phi, \\ \phi &= \begin{bmatrix} \phi_1 \\ \phi_2 \end{bmatrix} = \begin{bmatrix} B_1^T P x \\ B_2^T P x \end{bmatrix} = B^T P x \end{aligned} \tag{16}$$

where E_w=Diag(η_{11}, η_{21},…, η_{r1}, η_{12}, η_{22},…, η_{r2}).

2.3 Stability analysis

***Theorem 1*:** The following controller (17) enforces the error dynamics x to converge to zero.

$$u = -Kx + \mathrm{H} W \tag{17}$$

***Proof*:** Assume that (7) is feasible, and then there exists a matrix $Q > 0$ such that

$$X^{-1}[(A-BK)X + X(A-BK)^T]X^{-1} \le -Q < 0 \tag{18}$$

Let the Lyapunov function be chosen as

$$V = x^T P x + W_e^T E_w^{-1} W_e \tag{19}$$

where $W_e = W - W^*$. The time derivative of (19) along the error dynamics (4) is given by

$$\begin{aligned} \dot{V} &= 2x^T P \dot{x} + 2W_e^T E_w^{-1} \dot{W}_e \\ &= 2x^T P[Ax + B(u-f)] + 2W_e^T E_w^{-1} \dot{W} - 2W_e^T E_w^{-1} \dot{W}^* \\ &= 2x^T P[Ax + B(-Kx + \mathrm{H}W - \mathrm{H}W^*)] + 2W_e^T E_w^{-1} \dot{W} \\ &= 2x^T P[Ax + B(-Kx + \mathrm{H}W_e)] - 2W_e^T E_w^{-1} E_w \mathrm{H}^T \phi \\ &= 2x^T P(A-BK)x + 2x^T PB\mathrm{H}W_e - 2W_e^T \mathrm{H}^T \phi \\ &= 2x^T P(A-BK)x + 2\phi^T \mathrm{H}W_e - 2\phi^T \mathrm{H}W_e \\ &\le -x^T Q x < 0 \end{aligned} \tag{20}$$

Integrating both sides of (20) yields the following equation

$$\int_0^\infty x(\tau)^T Q x(\tau) d\tau = -\int_0^\infty \dot{V}(\tau) d\tau = V(0) - V(\infty) < \infty \tag{21}$$

This implies $x \in L_2 \cap L_\infty$ and $W \in L_\infty$. Using the above results and Barbalat's lemma, x asymptotically converges to zero as time approaches infinity.

***Remark 1*:** Note that the LMI parameterization of the K (8) can be combined with various useful convex performance criteria (i.e., α-stability, quadratic performance, generalized H_2/H_∞ performance, etc). For instance, if the K is given by (8) satisfying for some $\alpha > 0$, then

$$X > 0,\ AX - BY + XA^T - Y^T B^T + 2\alpha X < 0 \tag{22}$$

It implies that x converges to zero with a minimum decay rate α.

***Remark 2*:** Note that the NFC algorithm consists of layers, nodes in each layer, and online self-tuning algorithm. In general, the control performance can get better as the number of layers and nodes increases. However, this leads to a more complicated control system structure. Additionally, the updated laws for the parameters of all layers bring about a burdensome computation because of a large series of training data. Therefore, the structure and online self-tuning algorithm of the NFC should be designed simply and reasonably. For the proposed speed controller, the updated laws can be applied only to extract the parameters of the output layer. Besides, the parameters of the inner layer such as the standard deviation parameters of the membership functions can be selected as fixed parameters according to the control engineering knowledge. This solution still guarantees the stability criteria of the control system (20).

***Remark 3*:** This remark discusses how the controller gains are chosen. The proposed control law in (17) consists of the control term u_{fb} and the control term u_{nf}. The weights w_{ik} are integrated into the control term u_{nf} in (12). To attain the fast convergence and transient response, the weights w_{ik} are tuned to large values. As indicated in (15), these weights w_{ik} are proportional to the parameters η_{ik}, so the

large values of η_{ik} lead to those of w_{ik}. Meanwhile, the gain matrix K of the control term u_{fb} is achieved by solving the LMIs (7) or (22). Finally, the design parameters K and η_{ik} can be systematically tuned as follows:

Step 1: Solving the LMIs (7) or (22) yields the gain matrix K;

Step 2: Set η_{ik} to quite small values and then increase η_{ik} by a small amount;

Step 3: If the transient and steady-state performances are satisfactory, then this process is completed. Otherwise, return to *Step 2* above.

3. Disturbance observer design

The proposed control law in (17) requires the rotor angular acceleration information β which is usually unavailable. Based on *Definition 2*, the rotor angular acceleration information β can be directly obtained from the time derivative of the speed. However, this calculation method can be affected by its high-frequency noises. To avoid directly calculating the time derivative of the speed, the rotor angular acceleration β needs the knowledge of the disturbance $d_1(t)$. Thus, a simple disturbance observer is designed in this paper.

From the (1) and *assumption 2*, the disturbance observer can be established as

$$\begin{aligned} \dot{\hat{x}}_o &= A_o\hat{x}_o + L(y_o - C_o\hat{x}_o) + B_o u_o \\ \hat{d}_1(t) &= C_d\hat{x}_o \end{aligned} \tag{23}$$

where $L \in R^{2\times 1}$ is an observer gain matrix, and

$$\hat{x}_o = \begin{bmatrix} \hat{\omega} \\ \hat{d}_1(t) \end{bmatrix}, x_o = \begin{bmatrix} \omega \\ d_1(t) \end{bmatrix}, A_o = \begin{bmatrix} -k_2 & -k_3 \\ 0 & 0 \end{bmatrix}, B_o = \begin{bmatrix} 1 \\ 0 \end{bmatrix},$$
$$u_o = k_1 i_{qs} + k_{11} i_{ds} i_{qs},\ y_o = C_o x_o,\ C_o = [10],\ C_d = [01]$$

From (23) the error dynamics is expressed by

$$\dot{\bar{x}}_o = [A_o - LC_o]\bar{x}_o \tag{24}$$

where $\bar{x}_o = x_o - \hat{x}_o$.

***Theorem 2*:** Assume that the following LMI condition is feasible

$$P_o > 0,\ P_o A_o - Y_o C_o + A_o^T P_o - C_o{}^T Y_o^T < 0 \tag{25}$$

where $P_o \in R^{2\times 2}$ and $Y_o \in R^{2\times 1}$ are decision variables. Also, assume that the observer gain matrix L is calculated by

$$L = P_o^{-1} Y_o \tag{26}$$

Then, $\bar{x}_o$ exponentially goes to zero.

***Proof*:** Assume that (25) is feasible, and then there exists a matrix $Q_o > 0$ such that

$$P_o A_o - Y_o C_o + A_o^T P_o - C_o{}^T Y_o^T \le -Q_o < 0 \tag{27}$$

Let the Lyapunov function be defined as

$$V_o = \bar{x}_o^T P_o \bar{x}_o \tag{28}$$

The time derivative of (28) along the error dynamics (24) is represented by

$$\begin{aligned} \dot{V}_o &= 2\bar{x}_o^T (P_o A_o - P_o L C_o)\bar{x}_o \\ &= 2\bar{x}_o^T (P_o A_o - Y_o C_o)\bar{x}_o \le -\bar{x}_o^T Q_o \bar{x}_o < 0 \end{aligned} \tag{29}$$

It indicates that $\bar{x}_o$ is asymptotically stable.

Remark 4: Note that the LMI parameterization of the L (26) can be combined with various convex performance criteria (i.e., α-stability, quadratic performance, generalized H_2/H_∞ performance, etc). For example, if the L is computed by (26) satisfying with some $\alpha > 0$, then

$$P_o > 0,\ P_o A_o - Y_o C_o + A_o^T P_o - C_o{}^T Y_o^T + 2\alpha P_o < 0 \tag{30}$$

It means that $\bar{x}_o$ converges to zero with a minimum decay rate α.

Using the NFC and the disturbance observer above, a disturbance observer-based control law can be designed, thus the control inputs (V_{qs} and V_{ds}) can be expressed as

$$\begin{bmatrix} V_{qs} \\ V_{ds} \end{bmatrix} = \begin{bmatrix} k_1 k_6 & 0 \\ 0 & k_8 \end{bmatrix}^{-1} (u_{fb} + u_{nf}), \tag{31}$$

$$u_{fb} = -K\hat{x}, \tag{32}$$

$$u_{nf} = H\hat{W}, \tag{33}$$

$$\dot{\hat{W}} = -E_w \mathrm{H}^T B^T P \hat{x}, \tag{34}$$

$$\hat{x} = \begin{bmatrix} \omega_e & \hat{\beta} & i_{dse} \end{bmatrix}^T, \tag{35}$$

$$\hat{\beta} = k_1 i_{qs} - k_2 \omega + k_{11} i_{ds} i_{qs} - k_3 \hat{d}_1(t) \tag{36}$$

***Remark 5*:** The design procedure of the proposed observer-based NFC method can be generalized as follows:

Step 1*:* Solve the LMIs (25) or (30). Then obtain the observer gain (26) and construct the observer (23).

Step 2: Solve the LMIs (7) or (22). Then obtain the controller gain matrix K using the formula (8).

Step 3: Choose the membership functions of the speed, q-axis current, and d-axis current. Then, construct the matrix H using (10) and (11).

Step 4: Using *Remark 3*, choose the parameters η_{ik}, calculate the updated law (34), and construct the observer-

based neuro-fuzzy control term (33).

Step 5: Construct the observer-based control inputs (31) based on (32) and (33).

4. Performance Investigation by Simulation and Experimental Results

To demonstrate the effectiveness of the proposed observer-based NFC algorithm, simulation and experiment studies are realized on a prototype IPMSM with the following specifications: rated power P_{rated} = 390 W; p = 4; R_s = 2.48 Ω; L_{qs} = 114 mH; L_{ds} = 75 mH; λ_m = 0.193 V.sec/rad; J = 0.00015 kg.m^2; B = 0.0001 N.m.sec/rad.

Let us design a disturbance observer that guarantees the minimum decay rate $\alpha = 300$. By solving the LMI condition (30) and (26), the gain matrix L is calculated as

$$L = \begin{bmatrix} 1200.3 \\ -27.1 \end{bmatrix}$$

Next, let us design a speed controller that guarantees the minimum decay rate α = 70. By solving the LMI condition (22) and (8), the gain matrix K is achieved as

$$K = 10^4 \times \begin{bmatrix} 1.9507 & 0.0279 & 0.0 \\ 0.0 & 0.0 & 0.0074 \end{bmatrix}$$

As described in *Remark 2*, considering a trade-off between a simple implementation and a satisfactory performance, the fuzzy rules are selected as $r = 3 \times 2 \times 2 = 12$. That is, the membership functions for three input variables ($z_1 = \omega$, $z_2 = i_{qs}$, and $z_3 = i_{ds}$) are adopted as

$$\begin{aligned}
&m_{11} = m_{12} = m_{13} = m_{14} = e^{-(\omega-300)^2/300^2}, \\
&m_{15} = m_{16} = m_{17} = m_{18} = e^{-\omega^2/300^2}, \\
&m_{19} = m_{110} = m_{111} = m_{112} = e^{-(\omega+300)^2/300^2}, \\
&m_{21} = m_{22} = m_{25} = m_{26} = m_{29} = m_{210} = e^{-(i_{qs}-2)^2/2^2}, \\
&m_{23} = m_{24} = m_{27} = m_{28} = m_{211} = m_{212} = e^{-(i_{qs}+2)^2/2^2}, \\
&m_{31} = m_{33} = m_{35} = m_{37} = m_{39} = m_{311} = e^{-(i_{ds}-1)^2}, \\
&m_{32} = m_{34} = m_{36} = m_{38} = m_{310} = m_{312} = e^{-(i_{ds}+1)^2}
\end{aligned}$$

Then, this leads to the control term u_{nf} with

$$\mathrm{H} = \begin{bmatrix} h_1\, h_2 \ldots h_{12} & 0 & 0 \ldots & 0 \\ 0 & 0 \ldots & 0 & h_1\, h_2 \ldots h_{12} \end{bmatrix},$$

$$\dot{\hat{W}} = -E_w \mathrm{H}^T B^T P \hat{x},\ E_w = \eta_w I,\ \eta_w > 0$$

Fig. 2 shows the overall schematic diagram of a laboratory prototype IPMSM drive system which contains an IPMSM, a three-phase PWM inverter, an encoder, a

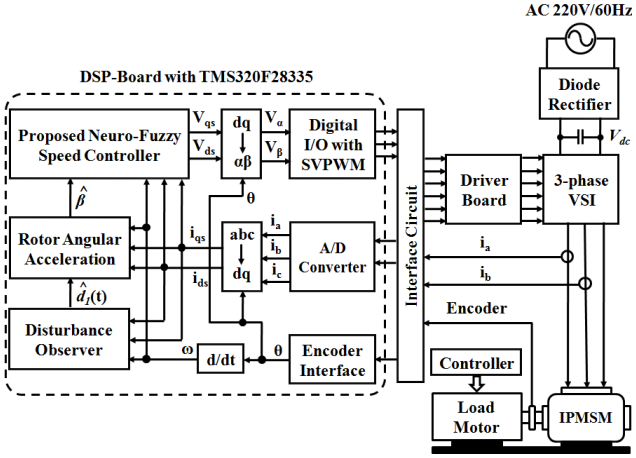

Fig. 2. Overall schematic diagram of a prototype IPMSM drive system.

control board with a TMS320F28335 DSP and load motor. The rotor position angle is measured through an encoder RIA-40-2500ZO, and the two stator currents (i_a, i_b) are detected via hall-effect current sensors. The three-phase stator current signals (i_a, i_b, i_c) are transformed to two-phase signals (i_{qs}, i_{ds}) in the dq reference frame. Meanwhile, the rotor angular acceleration information $\hat{\beta}$ is calculated via the disturbance observer, and then is provided for the proposed neuro-fuzzy speed controller. Considering the system efficiency, control performance and current ripples, the sampling and switching frequencies are chosen as 5 [kHz], and a space vector PWM (SVPWM) technique is employed. Furthermore, a servo IPMSM drive is used as a load motor to apply the load torque.

For a fair comparison, the observer-based FLC scheme in [2], which consists of the control structure similar to the proposed observer-based NFC algorithm, is adopted in this paper. The control inputs (V_{qs} and V_{ds}) are represented by

$$\begin{aligned}
&\begin{bmatrix} V_{qs} \\ V_{ds} \end{bmatrix} = \begin{bmatrix} k_1 k_6 + k_6 k_{11} i_{ds} & k_8 k_{11} i_{qs} \\ 0 & k_8 \end{bmatrix}^{-1} \begin{bmatrix} u_{fb1} + u_{ff} \end{bmatrix} \\
&u_{fb1} = -K_1 x_1,\ x_1 = \begin{bmatrix} \omega_e & \hat{\beta}_1 & i_{dse} \end{bmatrix}^T, \\
&\hat{\beta}_1 = -k_2 \omega + k_1 i_{qs} + k_{11} i_{ds} i_{qs} - k_3 \hat{T}_L, \qquad (37) \\
&K_1 = \begin{bmatrix} k_{11} & k_{12} & 0 \\ 0 & 0 & k_{23} \end{bmatrix},\ k_{11} > 0,\ k_{12} > 0,\ k_{23} > 0, \\
&u_{ff} = \begin{bmatrix} \left\{ k_2 \hat{\beta}_1 - (k_1 + k_{11} i_{ds})(-k_5 \omega - k_4 i_{qs} - k_{10} \omega i_{ds}) \right\} \\ -k_{11} i_{qs} (k_9 \omega i_{qs} - k_7 i_{ds}) \\ -k_9 \omega i_{qs} + k_7 i_{ds} \end{bmatrix}
\end{aligned}$$

where u_{fb1} is the state feedback term, u_{ff} is the feed forward term, and $\hat{T}_L$ is an estimate of T_L. The information of $\hat{T}_L$ is attained by constructing the load torque observer in [6]. For a fair comparison like [11], the gains of the proposed

NFC and the FLC methods are tuned to reach the similar speed response such as overshoot, settling time and error in steady-state under the nominal motor parameters. The proposed NFC scheme consists of the control terms u_{fb} and u_{nf}, while the FLC method consists of the control terms u_{fb1} and u_{ff}. It notes that the performance of the proposed NFC scheme depends on the gain matrix K of the u_{fb} and the parameters η_w of the u_{nf}, whereas that of the FLC scheme mainly depends on the gain matrix K_1 of the u_{fb1}. Additionally, the K and η_w can be easily tuned as in *Remark 3*. Meanwhile, the K_1 can be easily designed by using the pole placement technique. Consequently, the η_w of the proposed NFC strategy is adopted as 10,000, whereas the K_1 of the FLC method is elected as $k_{11} = 62{,}500$, $k_{12} = 500$, and $k_{23} = 3{,}000$.

Table 1. Case studies for simulations and experiments

Case	ω_d (*rad/s*)	T_L ($N{\cdot}m$)	Uncertainties
1	209.4 → –209.4	0.75	Nominal motor parameters
2	209.4 → –209.4	0.75	$\Delta R_s = +0.5R_s$, $\Delta L_{qs} = -0.3L_{qs}$ $\Delta L_{ds} = +0.1L_{ds}$, $\Delta\lambda_m = -0.2\lambda_m$
3	209.4 → –209.4	0.75	$\Delta J = +2.0J$, $\Delta B = +1.0B$
4	104.7	0.5 → 1.5	$\Delta J = +2.0J$, $\Delta B = +1.0B$

In this work, four case studies summarized in Table 1 are simulated using MATLAB/SIMULINK and tested to verify the feasibility of the proposed observer-based NFC scheme and the observer-based FLC scheme. *Cases 1* to *3* show the speed dynamic behaviors after a sudden change in the desired speed (ω_d), i.e., when the ω_d abruptly decreases from 209.4 [*rad/s*] to –209.4 [*rad/s*], but the T_L keeps 0.75 [$N{\cdot}m$]. Next, *Case 4* shows the torque dynamic behaviors after a sudden change in the load torque (T_L), i.e., when the T_L suddenly changes from 0.5 [$N{\cdot}m$] to 1.5 [$N{\cdot}m$], but the ω_d holds 104.7 [*rad/s*]. As presented in [24-25], the stator resistance (R_s) of the IPMSM varies as a function of the temperature, while the λ_m, L_{ds} and L_{qs} vary as a function of the operating current. The R_s increases as the temperature rises [24], and the λ_m and L_{qs} decrease as the i_{qs} increases [25]. However, the L_{ds} slightly increases as the i_{ds} is negative [25]. Furthermore, the J and B may strongly

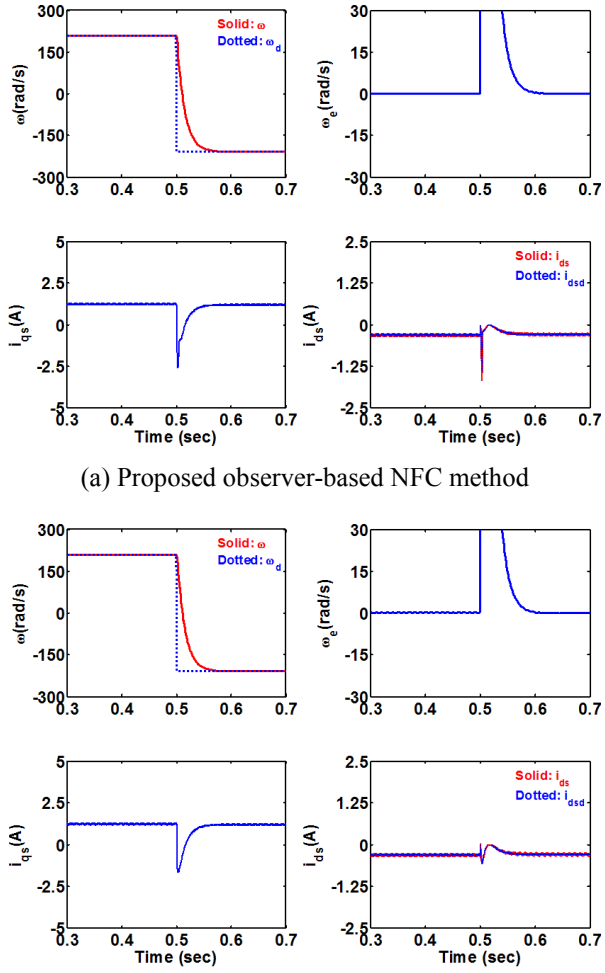

(a) Proposed observer-based NFC method

(b) Observer-based FLC method

Fig. 3. Simulation results of the proposed observer-based NFC method and the observer-based FLC method under *Case 1*.

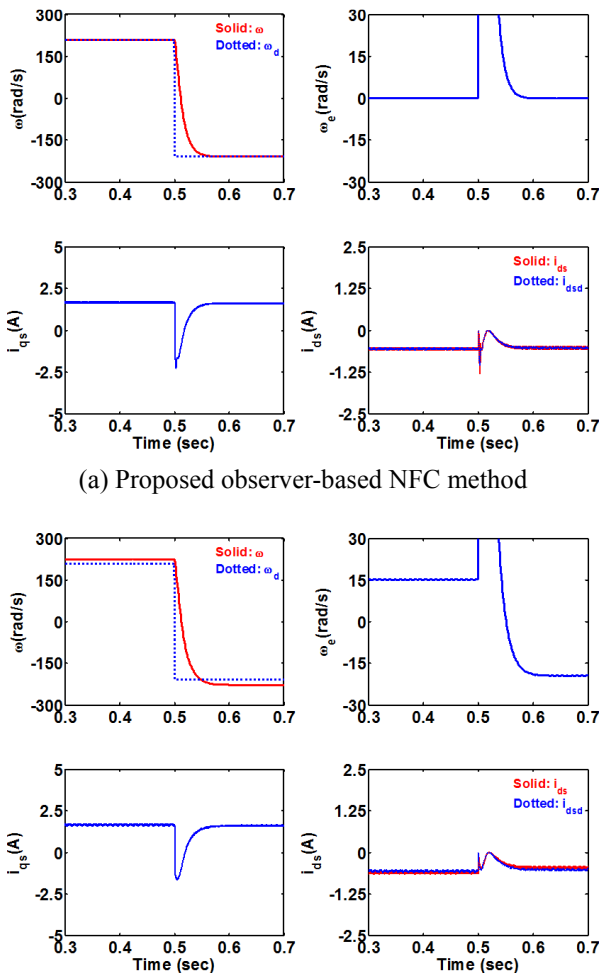

(a) Proposed observer-based NFC method

(b) Observer-based FLC method

Fig. 4. Simulation results of the proposed observer-based NFC method and the observer-based FLC method under *Case 2*.

increase as the external mechanical load is applied to the IPMSM drive. Thus, to demonstrate the robustness of the proposed observer-based NFC scheme, two kinds of parameter variations are given: *Case 2* is carried out under the electrical parameters variations (ΔR_s = +0.5R_s, ΔL_{qs} = –0.3L_{qs}, ΔL_{ds} = +0.1L_{qs}, $\Delta\lambda_m$ = –0.2λ_m) based on [24-25], whereas *Cases 3* and *4* are executed under the mechanical parameters variations (ΔJ = +2.0J, ΔB = +1.0B). It is well-known that the motor parameters can be easily adjusted in the simulation studies, but it is not an easy task to directly modify the motor parameters in the experiments. Generally, it can be an alternative solution to indirectly change the motor parameters in a real IPMSM drive by simply changing the motor parameters in the control scheme [9-10]. Thus, to conduct an experiment on the proposed observer-based control scheme under the variations of the motor parameters (R_s, L_{qs}, L_{ds}, λ_m, J, B), the motor parameters in the controller are indirectly changed rather than those in the real IPMSM drive.

Figs. 3(a)-5(a) show the speed step responses of the proposed NFC method under *Cases 1–3*, respectively, while Figs. 3(b)-5(b) show the speed step responses of the FLC method under *Cases 1–3*, respectively. Figs. 6(a) and 6(b) show the torque transient responses of both control methods under *Case 4*, respectively. In Figs. 3(a) and 3(b), the overshoot, the settling time and the steady-state error of the proposed NFC method and the FLC method are obtained under nominal motor parameters as (0.0%, 66 ms, 0.0%) and (0.0%, 65 ms, 0.03%), respectively. These results imply that the comparative evaluation was satisfactorily conducted and the FLC scheme can precisely track the speed reference trajectory of the IPMSM in case of the nominal motor parameters. In Figs. 4(a) and 4(b), it is observed that the speed errors in steady-state of both methods are almost zero and 4.67%, and the settling times are 57 [*ms*] and 69 [*ms*], respectively. Figs. 5(a) and 5(b) show that the undershoots of both control methods are

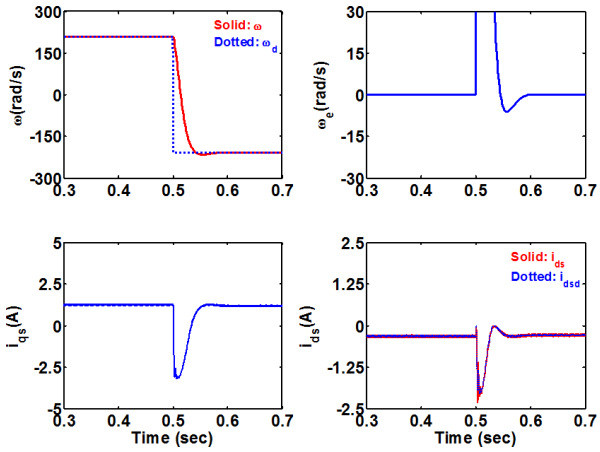

(a) Proposed observer-based NFC method

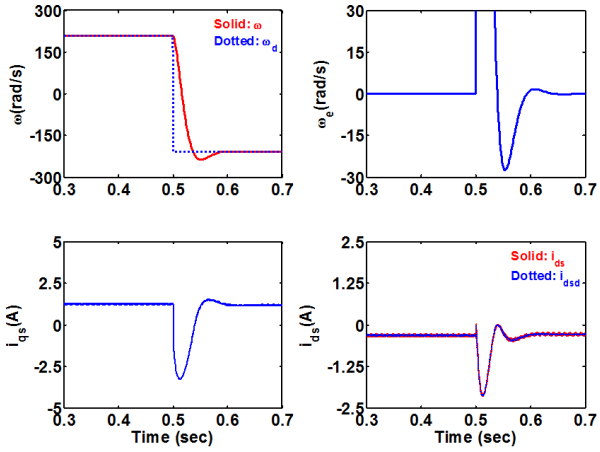

(b) Observer-based FLC method

Fig. 5. Simulation results of the proposed observer-based NFC method and the observer-based FLC method under *Case 3*.

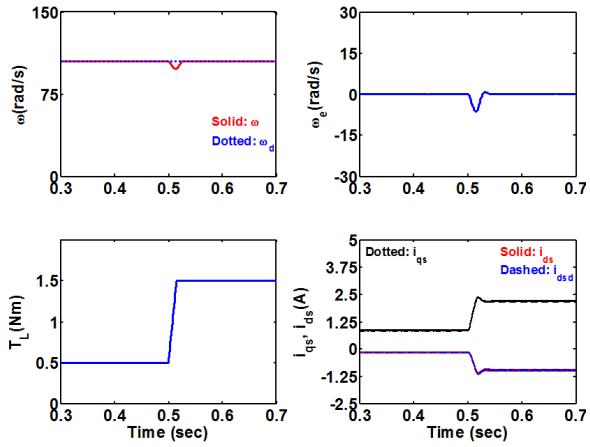

(a) Proposed observer-based NFC method

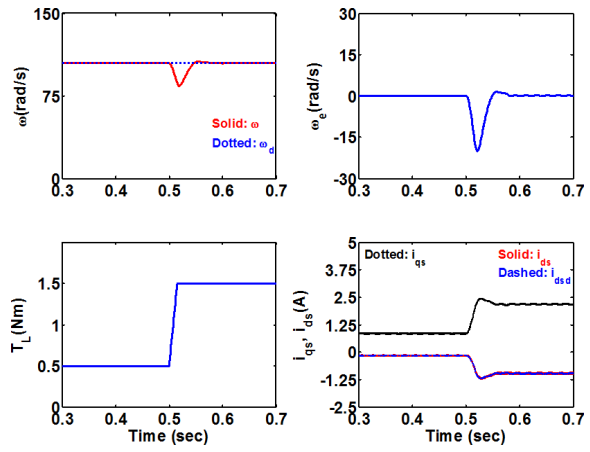

(b) Observer-Based Flc Method

Fig. 6. Simulation results of the proposed observer-based NFC method and the observer-based FLC method under *Case 4*.

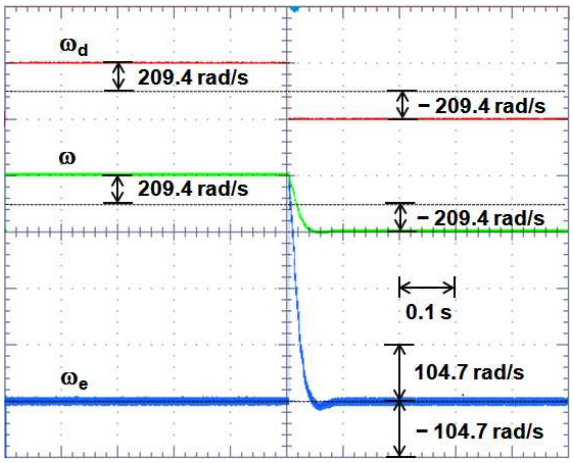

(a) ω_d, ω, and ω_e

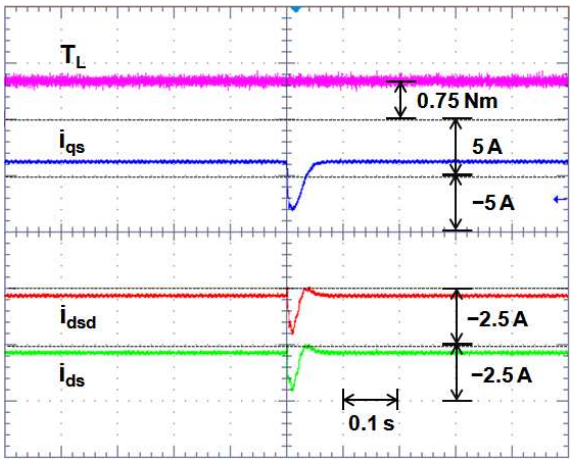

(b) T_L, i_{qs}, i_{dsd}, and i_{ds}

Fig. 7. Experimental results of the proposed observer-based NFC method under *Case 3*.

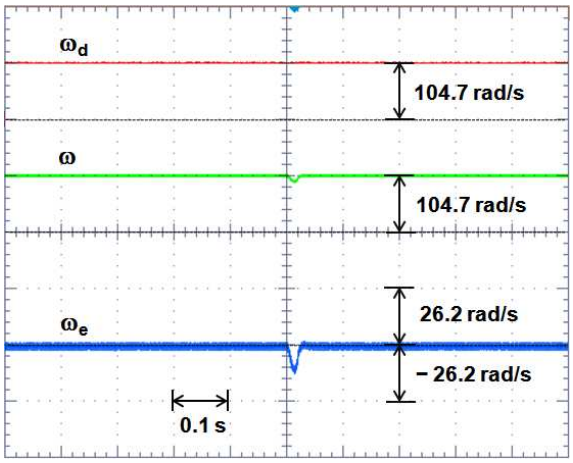

(a) ω_D, ω, AND ω_E

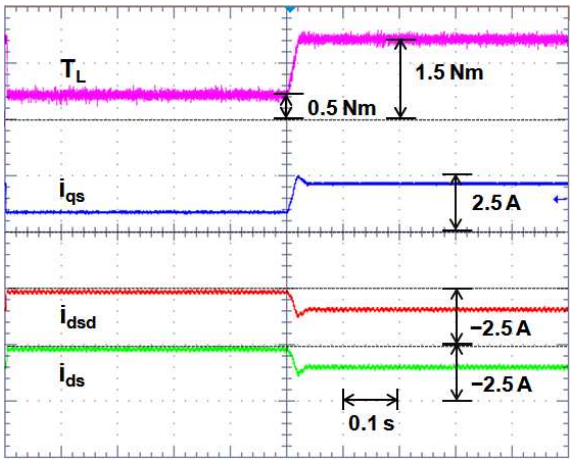

(b) T_L, I_{QS}, I_{DSD}, AND I_{DS}

Fig. 8. Experimental results of the proposed observer-based NFC method under *Case 4*.

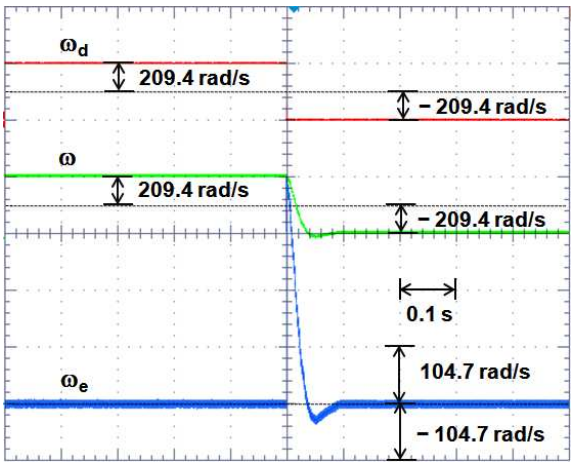

(a) ω_D, ω, AND ω_E

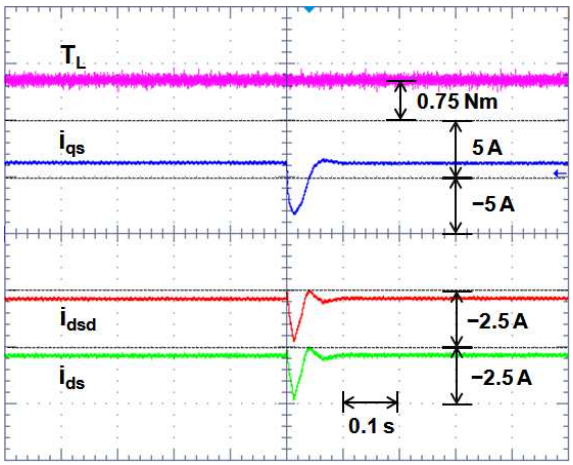

(b) T_L, I_{QS}, I_{DSD}, AND I_{DS}

Fig. 9. Experimental results of the observer-based FLC method under *Case 3*.

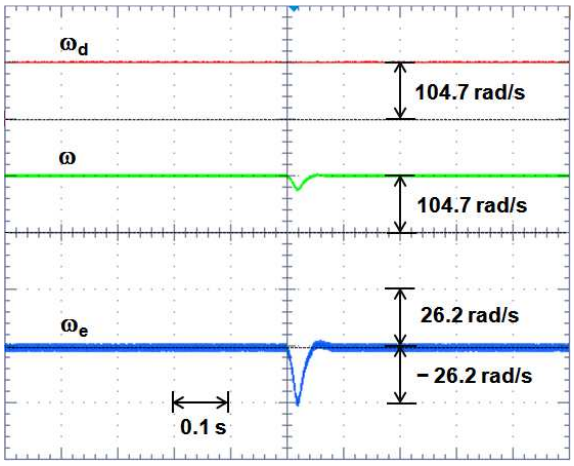

(a) ω_D, ω, AND ω_E

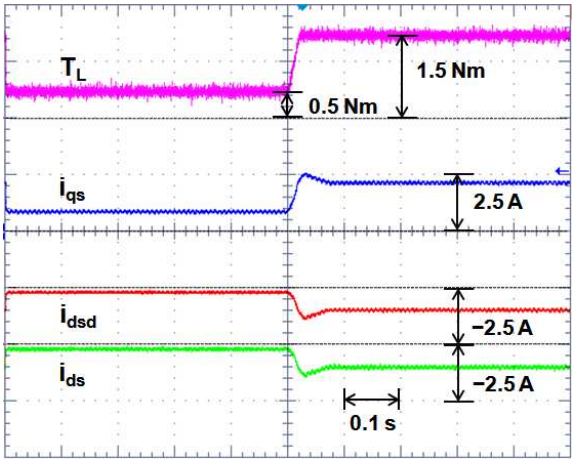

(b) T_L, I_{QS}, I_{DSD}, AND I_{DS}

Fig. 10. Experimental results of the observer-based FLC method under *Case 4*.

observed as 1.45% and 6.66%, and the settling times are 66 [*ms*] and 82 [*ms*], respectively. Figs. 6(a) and 6(b) show that the speed errors in steady-state are negligible, but the motor speed of Fig. 6(a) keeps much more stable than that of Fig. 6(b) during an abrupt load change.

In this work, *Cases 3* and *4*, which show the speed and torque transient responses under the mechanical parameters variations (ΔJ = +2.0J, ΔB = +1.0B), are chosen to experiment because of limited space. Figs. 7 and 8 show the experimental results of the proposed NFC method under *Cases 3* and *4*, respectively. Meanwhile, Figs. 9 and 10 show the test results of the FLC method under *Cases 3* and *4*, respectively. Table 2 summarizes the control performance of two control strategies during the transient and steady-state based on the simulation and experimental results.

From Figs. 3-10, it can be seen that the variations of the mechanical parameters (J, B) mainly affect the transient response. In fact, the variations of the electrical parameters

Table 2. Performance summaries of two control strategies during transient and steady-state based on simulation and experimental results

Case		Simulation		Experiment	
		Proposed NFC	FLC	Proposed NFC	FLC
Overshoot/ Undershoot (%)	*1*	0.0	0.0	0.0	0.0
	2	0.0	0.0	0.0	0.0
	3	1.45	6.66	2.05	7.85
	4	6.30	19.69	8.68	22.08
Settling Time (*ms*)	*1*	66	65	68	67
	2	57	69	60	74
	3	66	82	68	86
	4	22	42	25	47
Steady-State Error (%)	*1*	0.0	0.03	0.12	0.23
	2	0.0	4.67	0.18	6.07
	3	0.0	0.03	0.13	0.25
	4	0.03	0.30	0.24	0.95

(R_s, L_{qs}, L_{ds}, λ_m) slightly affect the steady-state response. Also, it is obvious that the proposed observer-based NFC scheme can obtain a better control performance (i.e., less steady-state error and more robustness) than the observer-based FLC scheme in case that some uncertainties in electrical and mechanical parameters exist.

5. Conclusion

In this work, a disturbance observer-based NFC methodology of a servo IPMSM drive system has been proposed. The proposed observer-based speed controller is insensitive to uncertain factors such as motor parameter variations and load torque disturbances. Additionally, the maximum torque per ampere (MTPA) control was incorporated to improve the torque generator in the constant torque region. In this study, the global stability analysis is comparatively simple and systematic since the time derivative of the quadratic Lyapunov function is elected as the cost function to be minimized. Moreover, the design procedure of the online self-tuning algorithm is simplified to reduce a computational burden of the NFC. Simulation and experimental results surely show that the proposed observer-based NFC scheme has a better speed tracking performance such as less steady-state error, more robustness than the observer-based FLC method in the existence of the uncertainties in electrical parameters and mechanical parameters.

Acknowledgements

This work was supported by the National Research Foundation of Korea (NRF) grant funded by the Korea government (MSIP) (No. 2012R1A2A2A01045312).

References

[1] V. Q. Leu, H. H. Choi, and J. W. Jung, "LMI-based sliding mode speed tracking control design for surface-mounted permanent magnet synchronous motors," *J. Elect. Eng. Technol*., Vol. 7, No. 4, pp. 513-523, Jul. 2012.

[2] Y. H. Kim, W. K. Kim, and S. Kim, "Maximum power control of IPMSM considering nonlinear cross-magnetization effects," *J. Elect. Eng. Technol*., Vol. 7, No. 6, pp. 940-947, Nov. 2012.

[3] H. Lin, K. Y. Hwang, and B. I. Kwon, "An improved flux observer for sensorless permanent magnet synchronous motor drives with parameter identification," *J. Elect. Eng. Technol*., Vol. 8, No. 3, pp. 516-523, May 2013.

[4] M. Sekour, K. Hartani, A. Draou, and A. Allali, "Sensorless fuzzy direct torque control for high performance electric vehicle with four in-wheel motors," *J. Elect. Eng. Technol*., Vol. 8, No. 3, pp. 530-543, May 2013.

[5] R. S. Rebeiro and M. N. Uddin, "Performance analysis of an FLC-based online adaptation of both hysteresis and PI controllers for IPMSM drive," *IEEE Trans. Ind. Appl.,* Vol. 48, No. 1, pp. 12-19, Jan./Feb. 2012.

[6] C. K. Lin, T. H. Liu, and S. H. Yang, "Nonlinear position controller design with input-output linearisation technique for an interior permanent magnet synchronous motor control system," *IET Power. Electron.,* Vol. 1, No. 1, pp. 14-26, Mar. 2008.

[7] M. A. Rahman, M. D. Vilathgamuwa, M. N. Uddin, and K. J. Tseng, "Nonlinear control of interior permanent-magnet synchronous motor," *IEEE Trans. Ind. App.,* Vol. 39, No. 2, pp. 408-416, Mar./Apr. 2003.

[8] S. Wu, Y. Wang, and S. Cheng, "Optimal reset control design for current control and uncertainties estimation in permanent magnet synchronous," *IET Electr. Power. Appl.,* Vol. 6, No. 2, pp. 122-132, Feb. 2012.

[9] R. Errouissi, M. Ouhrouche, W. H. Chen, and A. M. Trzynadlowski, "Robust cascaded nonlinear predictive control of a permanent magnet synchronous motor with antiwindup compensator," *IEEE Trans. Ind. Electron.,* Vol. 59, No. 8, pp. 3078-3088, Aug. 2012.

[10] R. Errouissi, M. Ouhrouche, W. H. Chen, and A. M. Trzynadlowski, "Robust nonlinear predictive controller for permanent magnet synchronous motors with an optimized cost function," *IEEE Trans. Ind. Electron.,* Vol. 59, No. 7, pp. 2849-2858, Jul. 2012.

[11] H. Chaoui and P. Sicard, "Adaptive fuzzy logic control of permanent magnet synchronous machines with nonlinear friction," *IEEE Trans. Ind. Electron.,* Vol. 59, No. 2, pp. 1123-1133, Feb. 2012.

[12] M. N. Uddin and R. S. Rebeiro, "Online efficiency optimization of a fuzzy logic controller-based IPMSM drive," *IEEE Trans. Ind. App.,* Vol. 47, No. 2, pp. 1043-1050, Mar./Apr. 2011.

[13] G. Foo and M. F. Rahman, "Sensorless sliding-mode MTPA control of an IPM synchronous motor drive using a sliding mode observer and HF signal injection," *IEEE Trans. Ind. Electron.,* Vol. 57, No. 4, pp. 1270-1278, Apr. 2010.

[14] C. K. Lin, T. H. Liu, M. Y. Wei, L. C. Fu, and C. F. Hsiao, "Design and implementation of a chattering-free nonlinear sliding mode controller for interior permanent magnet synchronous drive systems," *IET Electr. Power. Appl.,* Vol. 6, No. 6, pp. 332-344, Jul. 2012.

[15] K. Liu, Z. Q. Zhu, and D. A. Stone, "Parameter estimation for condition monitoring of PMSM stator winding and rotor permanent magnets," *IEEE Trans. Ind. Electron.,* Vol. 60, No. 12, pp. 5902-5913, Dec. 2013.

[16] Y. Feng, X. Yu, and F. Han, "High-order terminal sliding-mode observer for parameter estimation of a permanent-magnet synchronous motor," *IEEE Trans. Ind. Electron.,* Vol. 60, No. 10, pp. 4272-4280, Oct. 2013.

[17] M. Tursini, F. Parasiliti, and D. Zhang, "Real-time gain tuning of PI controllers for high-performance PMSM drives," *IEEE Trans. Ind. App.,* Vol. 38, No. 4, pp. 1018-1026, Jul./Aug. 2002.

[18] M. N. Uddin, M. A. Abido, and M. A. Rahman, "Development and implementation of a hybrid intelligent controller for interior permanent magnet synchronous motor dives," *IEEE Trans. Ind. App.,* Vol. 40, No. 1, pp. 68-76, Jan./Feb. 2004.

[19] M. Khan and M. A. Rahman, "Implementation of a new wavelet controller for interior permanent magnet motor drives," *IEEE Trans. Ind. App.,* Vol. 44, No. 6, pp. 1957-1965, Nov./Dec. 2008.

[20] M. M. I. Chy and M. N. Uddin, "Development and implementation of a new adaptive intelligent speed controller for IPMSM drive," *IEEE Trans. Ind. App.,* Vol. 45, No. 3, pp. 1106-1115, May/Jun. 2009.

[21] M. A. S. K. Khan and M. A. Rahman, "A novel neuro wavelet-based self tuned wavelet controller for IPM motor drives," *IEEE Trans. Ind. App.,* Vol. 46, No. 3, pp. 1194-1203, Mar. 2010.

[22] F. F. M. El-Sousy, "Robust adaptive H^{∞} position control via a wavelet neural network for a DSP-based permanent magnet synchronous motor servo drive system," *IET Electr. Power. Appl.,* Vol. 4, No. 5, pp. 333-347, May 2010.

[23] F. F. M. El-Sousy, "Robust wavelet neural network sliding mode control system for permanent magnet synchronous motor drive," *IET Electr. Power. Appl.,* Vol. 5, No. 1, pp. 113-132, Feb. 2011.

[24] F. Fernandez-Bernal, A. Garcia-Cerrada, and R. Faure, "Determination of parameters in interior permanent-magnet synchronous motors with iron losses without torque measurement," *IEEE Trans. Ind. App.,* Vol. 37, No. 5, pp. 1265-1272, Sep./Oct. 2001.

[25] P. H. Mellor, M. A. Al-Taee, and K. J. Binns, "Open loop stability characteristics of synchronous drive incorporating high field permanent magnet motor," *IEE Proceedings-B,* Vol. 138, No. 4, pp. 175-184, Jul. 1991.

Dong Quang Dang received the B.S. and M.S. degrees in Electrical Engineering from Hanoi University of Science and Technology (HUST), Hanoi, Vietnam in 2005 and 2010, respectively. From 2006 to 2011, he worked at Hung Yen University of Technology and Education, Hung Yen, Vietnam, as a lecturer. He is currently pursuing the Ph.D. degree in the Division of Electronics and Electrical Engineering, Dongguk University, Seoul, Korea. His research interests are in the field of electric machine drives and control of distributed generation systems using renewable energy sources.

Nga Thi-Thuy Vu received the B.S. and M.S. degrees in Electrical Engineering from Hanoi University of Science and Technology (HUST), Hanoi, Vietnam in 2005 and 2008, respectively, and the Ph.D degree in Electronics and Electrical Engineering, Dongguk University, Seoul, Korea, in 2013. Currently, she is with the Department of Automation Control, Hanoi University of Science and Technology as a full lecturer. Her research interests are in the field of DSP-based electric machine drives and control of distributed generation systems using renewable energy sources.

Han Ho Choi received the B.S. degree in Control and Instrumentation Engineering from Seoul National University, Seoul, Korea, in 1988, and the M.S. and Ph.D. degrees in Electrical Engineering from Korea Advanced Institute of Science and Technology (KAIST), Daejeon, Korea, in 1990 and 1994, respectively. From 1994 to 1998, he was a Team Leader with the Advanced Technology Laboratory, DaeWoo Electrical Co., Ltd., Korea. He is currently with the Division of Electronics and Electrical Engineering, Dongguk University, Seoul, Korea. His research interests include linear-matrix-inequality-based control system design, microprocessor-based control systems, variable-structure systems, and microprocessor-based electric machine drives.

Jin-Woo Jung received the B.S. and M.S. degrees in Electrical Engineering from Hanyang University, Seoul, Korea in 1991 and 1997, respectively, and the Ph.D. degree in Electrical and Computer Engineering from The Ohio State University, Columbus, Ohio, USA, in 2005. From 1997 to 2000, he was with the Home Appliance Research Laboratory, LG Electronics Co., Ltd., Seoul, Korea. From 2005 to 2008, he was a Senior Research Engineer with the R&D Center and PDP Development Team, Samsung SDI Co., Ltd., Korea. Since 2008, he has been an Associate Professor with the Division of Electronics and Electrical Engineering, Dongguk University, Seoul, Korea. His current research interests are in the area of DSP-based electric machine drives, power conversion circuit design and control algorithm for electric vehicles (EV), control of distributed generation systems (DGS) using renewable energy sources (wind turbines/fuel cells, solar cells), and driving circuits and driving methods of ac plasma display panels (PDP) and liquid crystal displays (LCD).